

# Journal of Geophysical Research: Atmospheres

## RESEARCH ARTICLE

10.1002/2016JD024835

**Key Points:**

- All-time record heat in Santiago Chile (130 year record) is analyzed
- Forcing mechanisms for extreme rainfall in Atacama Desert are explored
- Extreme rainfall in Atacama found related to extreme heat in central Chile

**Correspondence to:**B. S. Barrett,  
bbarrett@usna.edu**Citation:**Barrett, B. S., D. A. Campos, J. Vicencio Veloso, and R. Rondanelli (2016), Extreme temperature and precipitation events in March 2015 in central and northern Chile, *J. Geophys. Res. Atmos.*, 121, doi:10.1002/2016JD024835.

Received 20 JAN 2016

Accepted 16 APR 2016

Accepted article online 20 APR 2016

## Extreme temperature and precipitation events in March 2015 in central and northern Chile

**Bradford S. Barrett<sup>1</sup>, Diego A. Campos<sup>2,3,4</sup>, José Vicencio Veloso<sup>5</sup>, and Roberto Rondanelli<sup>2,6</sup>**

<sup>1</sup>Oceanography Department, U.S. Naval Academy, Annapolis, Maryland, USA, <sup>2</sup>Department of Geophysics, University of Chile, Santiago, Chile, <sup>3</sup>Centro Nacional del Medio Ambiente, Universidad de Chile, Santiago, Chile, <sup>4</sup>Aplicaciones Satelitales, Dirección Meteorológica de Chile, Santiago, Chile, <sup>5</sup>Meteorología Agrícola, Dirección Meteorológica de Chile, Santiago, Chile, <sup>6</sup>Center for Climate and Resilience Research, (CR)2, Santiago, Chile

**Abstract** From 18 to 27 March 2015, northern, central, and southern Chile experienced a series of extreme hydrometeorological events. First, the highest surface air temperature ever recorded in Santiago (with reliable records dating to 1877), 36.8°C at Quinta Normal, was measured at 15:47 local time on 20 March 2015. Immediately following this high heat event, an extreme precipitation event, with damaging streamflows from precipitation totals greater than 45 mm, occurred in the semiarid and hyperarid Atacama regions. Finally, concurrent with the heavy precipitation event, extremely warm temperatures were recorded throughout southern Chile. These events were examined from a synoptic perspective with the goal of identifying forcing mechanisms and potential interaction between each analysis which provides operational context by which to identify and predict similar events in the future. Primary findings were as follows: (1) record warm temperatures in central Chile resulted from anomalous lower troposphere ridging and easterly downslope flow, both of which developed in response to an anomalous midtroposphere ridge-trough pattern; (2) a cutoff low with anomalous heights near one standard deviation below normal slowly moved east and was steered ashore near 25°S by circulation around a very strong ridge (anomalies more than 3 standard deviations above normal) centered near 60°S; (3) anomalously high precipitable water content (20 mm above climatological norms) over the Peruvian Bight region was advected southward and eastward ahead of the cutoff low by low-level northwesterly flow, greatly enhancing observed precipitation over northern Chile.

### 1. Introduction

During the second half of March 2015, extreme warm surface temperature anomalies were registered in central, southern, and austral Chile, even reaching to the Antarctic continent. Four days later, very heavy precipitation fell in the northern region of the country affecting the hyperarid and semiarid parts of the Atacama Desert, generating floods, alluviums, and destruction in several towns. In this paper, we analyze the synoptic-scale conditions present in Chile, South America, and upstream in the Southeast Pacific, from 18 to 27 March 2015, during which both events occurred.

Extreme surface air temperature events in Chile are important hydrometeorologically because of their connection to evaporation, long-term drought, and air column stability. Over western North America, extreme heat events are typically 3 days or longer [Grotjahn and Faure, 2008; Bumbaco et al., 2013] and result from displacement of a hot air mass that can readily be seen as anomalies in both geopotential height and wind fields [Grotjahn, 2016]. For California (a region that can be considered analogous to central Chile), hottest surface temperatures are generally seen when two conditions are met: first, upper troposphere temperatures need to be above normal, and warmer temperatures aloft often occur concurrently with subsidence, clear skies, a temperature inversion located closer to the surface, and warmer air temperatures in the boundary layer; second, surface low pressure needs to be present at the coast, and circulation around this low will drive local downslope conditions and oppose sea breeze formation [Hughes and Hall, 2010]. Heat events like this can be deadly to the local population, particularly among vulnerable populations. For example, in Santiago, Bell et al. [2008] found a 2.7% increase in mortality of elderly population (65 years old or older) when mean daily temperatures exceeded the 95th percentile. Muggeo and Hajat [2009] noted an increase in all-cause mortality of 5.5% among the same population. Hence, understanding the synoptic-scale characteristics of the record heat event of March 2015 has important societal implications.

Understanding the synoptic-scale characteristics of the record precipitation event of March 2015 also has important societal implications, particularly considering that it occurred in one of the driest regions of the

continent. The region between 18.4°S and about 26°S comprises the hyperarid Atacama Desert [Garreaud and Aceituno, 2007; Schulz et al., 2012], with annual mean of less of 1.7 mm of rainfall [Ruttlant et al., 2003]. Between 26°S and 31°S, precipitation becomes more frequent and the Atacama slowly transitions from hyperarid to semiarid, due to more frequent winter cold frontal passages [e.g., Barrett et al., 2009]. The entire Atacama, both hyperarid north and semiarid south, falls under the effects of the South East Pacific Anticyclone (SEPA) [Muñoz and Garreaud, 2005; Klein and Hartmann, 1993; Ma et al., 1996; Stephens, 2005; Rahn and Garreaud, 2010; Mechoso et al., 2014], which generates subsidence and generally blocks convective precipitation [Garreaud and Aceituno, 2007]. Wintertime frontal activity is also minimized, especially north of about 25°S, when compared to central and southern Chile, again due to the persistent SEPA over the ocean [Garreaud, 2009; Valdés-Pineda et al., 2015]. However, in instances when the SEPA shifts, changes intensity, or is undercut by cutoff low systems, precipitation is possible [Meza, 2013].

Cutoff low systems over the subtropical Pacific Ocean are relatively common features of the synoptic meteorology of South America. In the upper troposphere, these lows develop from preexisting troughs that separate from their connection with the polar source region [Nieto et al., 2008; Gimeno et al., 2007]. Through quasi-geostrophic mechanisms, the upper level cutoff low sometimes promotes surface cyclogenesis [e.g., Hakim, 2003]. Over southern South America, including Chile, the most frequent seasons for cutoff low formation are austral autumn (March–May) [Campetella and Possia, 2007] or austral winter (June–August) [Reboita et al., 2010]. Most cutoff low events last 2 to 3 days and progress eastward. Cutoff lows are important to the regional climate because they often bring precipitation [Fuenzalida et al., 2005], physically doing so by deepening the boundary layer and increasing near-surface moisture advection [Rahn, 2014]. Because they are associated with cold air aloft, as they progress over the relatively warmer ocean, the air column can become statically unstable and lead to deep convection and heavy precipitation [Nieto et al., 2005; Miky-Funatsu et al., 2004]. Indeed, between 20 and 40% of the annual precipitation between 28°S and 32°S can be attributed to cutoff lows (C. Barahona, personal communication, 2015), a value that decreases to between 5 and 10% per year by 36°S [Pizarro and Montecinos, 2000]. Because precipitation equatorward of 28°S is relatively rare, it is unclear what fraction of precipitation over the Atacama might be related to cutoff lows.

Most of the historical rainfall events in the coast and valleys from the Antofagasta to Coquimbo regions (21°S–32°S) occur during the winter time. However, some events are also associated with cutoff lows, and these have been observed in both winter and summer. For example, the extreme precipitation event in the Río Copiapó catchment of June 1997 (27.7°S, 70.2°W) featured more than 92 mm of rainfall in 24 h, estimated to be a near 61 year event [Märker et al., 2012]. This event featured a cutoff low centered near 45°S. As a summer example, in February 2001, heavy rainfall along the elevated Andes cordillera associated with a deep trough resulted in severe flooding in the Río Loa (21.2°S, 68.7°W), which inundated the northern town of Calama [Houston, 2006]. Instantaneous peak flow in a tributary of Río Loa reached  $310 \text{ m}^3 \text{ s}^{-1}$ , more than an order of magnitude higher than ever observed before. Similar to the event of March 2015, heavy precipitation in these arid regions quickly produces damaging landslides and alluviums in the valleys and coast. Indeed, the city of Antofagasta saw seven such landslide events during the June-to-August period in the twentieth century [Vargas et al., 2000], and Urrutia and Lanza [1993] documented six events in north-central Chile in February and March between 1800 and 1992.

In addition to the unusual nature of the cutoff low in this study (it formed early in the season and along 25°S, an unusually equatorward latitude for South American cutoff lows in late summer or early autumn; [Fuenzalida et al., 2005]), the low happened to follow in the wake of a heat wave-producing upper troposphere ridge over the continent. The temporal juxtaposition of these two extreme events was unique: in the span of only 1 week, central Chile experienced record-breaking temperatures and northern Chile experienced extreme precipitation. Given this close proximity in both time and space, it is likely that the two events were connected, a hypothesis that was tested in this study.

The primary goal of the paper is to provide a synoptic-scale analysis of these rare but hazardous events. By identifying the characteristics and forcing mechanisms for both the temperature and precipitation extremes, events which have important disaster management implications [e.g., Middleton and Sternberg, 2013], our analysis provides operational meteorologists and forecasters context by which to identify and predict future extreme events. We also fill a gap in the current literature; we do not know of any studies prior to this one have examined extreme heat in Chile or connected it to extreme precipitation in the Chilean Atacama. The

**Table 1.** Datasets, Date Ranges, and Number of Stations (or Resolution) Used in This Study

Variable	Data Set	Date Ranges	Number of Stations (or Data Set Resolution)
Daily maximum air temperature (at 2 m, in °C)	Dirección Meteorológica de Chile (DMC)	18–27 March 2015	16 surface stations
Relative frequency and rank, daily maximum air temperature	Dirección Meteorológica de Chile (DMC)	15–30 March 1950–2015 (1952–2015 for La Serena)	9 surface stations
Air temperature forecasts	GFS predictions, 3-hourly out to 172 h	Forecasts initialized every 6 h between 0000 UTC 17 March 2015 and 1800 UTC 22 March 2015	0.5° horizontal resolution
Height (500 hPa; in m), wind (500 hPa, 850 hPa; in $m s^{-1}$ ), sea level pressure (in hPa), temperature (850 hPa; in °C), precipitable water (in mm)	GFS FNL analyses	Analyses at 1200 UTC daily between 19 March 2015 and 26 March 2015	0.5° horizontal resolution
Upper air temperature and dew point temperature (both in °C), height (in m), and wind speed (in $m s^{-1}$ ) and direction	Integrated Global Radiosonde Archive (IGRA), from NOAA National Centers for Environmental Information	1200 UTC (0900 local), 19–26 March 2015	4 upper air stations
Precipitation (in mm)	Dirección Meteorológica de Chile (DMC), Dirección General de Aguas (DGA), and Sistema de Red Agroclima	23–27 March 2015	46 surface stations
Infrared brightness temperatures	GOES East	Daily at 1700 UTC (1400 local) between 21 and 26 March	4 km horizontal resolution
Precipitation accumulated (in mm)	TRMM 3B42	20–27 March 2015	0.25° longitude × 0.25° latitude resolution
Streamflow (in $m^3 s^{-1}$ ) and rainfall (in mm (3 h) $^{-1}$ )	Dirección General de Aguas (DGA)	3-hourly observations between 19 and 27 March 2015	3 stations

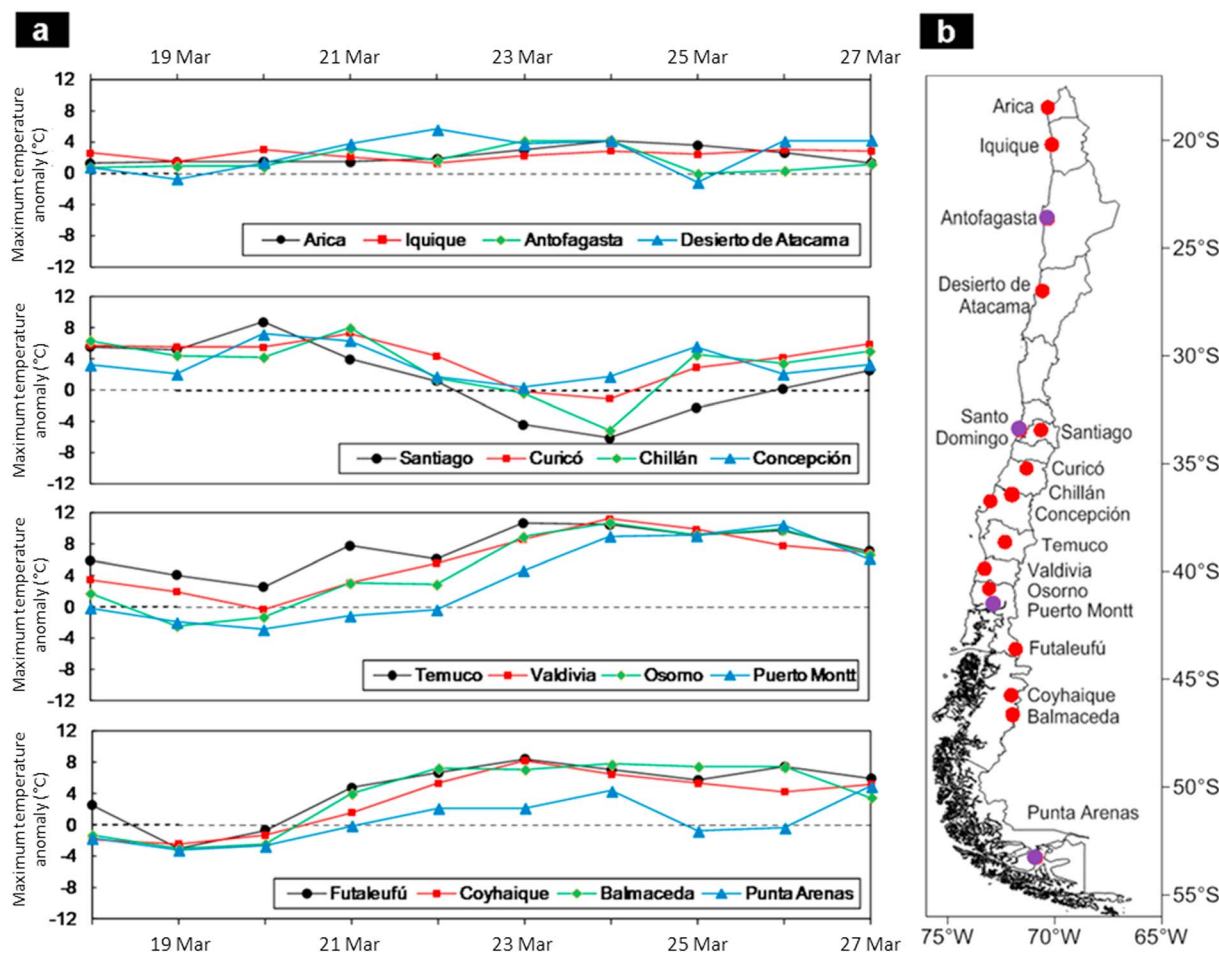


**Figure 1.** Daily anomalies of maximum temperature (in °C), from (a) 18 to 27 March 2015. Anomalies calculated with respect to the 1981–2010 March mean. Data are from observations maintained by the Dirección de Meteorología de Chile (DMC). (b) Locations of the temperature and upper air stations used in the analysis. Purple circles were used to indicate the radiosonde station stations referenced in Figure 7.

paper is organized chronologically, starting with the record warm temperatures in central Chile that peaked around 20 March 2015, and then analyzing the development of the cut off low and extreme precipitation that peaked around 24 March 2015. The remainder of this paper is organized as follows. In section 2, data and methods are presented. A summary of the extreme heat event is presented in section 3.1, and in section 3.2, the heavy precipitation event is analyzed. A discussion of the two events, as well as conclusions from both, is presented in section four.

## 2. Data and Methods

Surface, satellite, model, and reanalysis data sets were used in this analysis (see Table 1 for details of each data set). Daily maximum surface air temperatures at 16 observing stations across Chile, from Arica in the north to Punta Arenas in the south (stations indicated in Figure 1b), were examined over the period 18 to 27 March 2015 (data from the Dirección Meteorológica de Chile, DMC). Anomalies of daily maximum air temperatures were calculated for each of the 16 stations by subtracting the March 1981–2010 mean from the observed maximum air temperatures. To put the daily maximum surface air temperatures in historical perspective, relative frequencies for nine of the stations were calculated for maximum temperatures during the second 15 day period (days 15–30) of March, from 1950 to 2015 (1952–2015 for La Serena) (data also from the DMC). Ranks of the observed maximum temperatures during the heat event were also calculated from these historical observations. Event total rainfall was analyzed from 23 to 27 March 2015 for 46 precipitation measuring stations, maintained by both the DMC and the Dirección General de Aguas (DGA), between 18°S and 38°S. The

pattern of observed daily rainfall totals was compared to rainfall totals over consecutive 24 h periods between 20 and 27 March 2015 using daily accumulated precipitation totals from the Tropical Rainfall Measuring Mission (TRMM) 3B42 version 7 data set. The TRMM data have some biases and underestimates, particularly in regions of varied topography [e.g., *Tian et al.*, 2007; *Dinku et al.*, 2009], but (as shown in the next section) TRMM observations qualitatively agreed with both the timing and spatial distribution of observations from surface stations. Streamflow data from DGA for three stations was examined from 19 to 27 March 2015. Infrared satellite brightness temperatures from Geostationary Operational Environmental Satellite (GOES East) were examined from 21 to 26 March 2015. Daily vertical profiles of temperature and dew point temperature at four upper air observing sites in Chile (Antofagasta, Santo Domingo, Puerto Montt, and Punta Arenas, indicated by points on Figure 1b) from the NOAA Integrated Global Radiosonde Archive (IGRA, available at <ftp://ftp.ncdc.noaa.gov/pub/data/igra>) at 1200 UTC (0900 local) were examined. Additionally, point values of geopotential height and zonal wind at 925, 850, and 500 hPa from the NOAA Earth System Research Laboratory radiosonde database were examined. Gridded values of geopotential height at 500 hPa,  $u$  and  $v$  wind components at 500 and 850 hPa, temperature at 850 hPa, total column precipitable water, 2 m temperature, and sea level pressure were taken from the National Centers for Environmental Prediction (NCEP) Global Forecast System (GFS) 0 h analyses, available every 6 h with 0.5° horizontal resolution (available in real time from <ftp://ftp.ncep.noaa.gov/pub/data/nccf/com/gfs/prod>). Forecasts of 2 m temperature at 3 h intervals were taken from GFS forecasts [*Caplan et al.*, 1997] initialized every 6 h from 0000 UTC 17 March 2015 through 1800 UTC 22 March 2015. Predictions of 2 m temperature for the Santiago metropolitan region ( $33.5^{\circ}\text{S}$ ,  $70.5^{\circ}\text{W}$ ) at 3 h intervals initialized at synoptic times (0000, 0600, 1200, and 1800 UTC) starting at 0000 UTC 17 March 2015. Anomalies of 500 hPa height and wind, 850 hPa temperature and wind, precipitable water, and sea level pressure were calculated by subtracting the NCEP-National Center for Atmospheric Research Reanalysis II 1981–2010 March mean from GFS analyses.

These different data sets were selected because together they provide both physical and historical context to the extreme temperature and precipitation. It is important to note that the data sets have different temporal periods, including different periods over which anomalies were calculated. A disadvantage to this approach is that the temporal record is nonstationary, as the presence of various scales of motion in the different time series complicates the interpretation of long-term trends in the meteorological variables [*Eskridge et al.*, 1997]. However, an advantage to this approach is that all available data were used, providing the most complete historical context possible.

### 3. Results

The temperature and precipitation events of 18–27 March 2015 in Chile were notable for their extremity: all-time record high temperatures (in the instrument record) were set in central Chile, including Santiago the capital, where instrument records extend back to 1877, and rainfall records and flooding in the arid north of Chile. The events will be considered chronologically, with the extreme heat in central Chile examined first, followed by the extreme precipitation in northern Chile. In addition, notable positive surface and lower troposphere temperature anomalies were seen in south-central and southern Chile, concurrent with the cutoff low and heavy precipitation in the north, and these will also be examined.

#### 3.1. Extreme Temperatures

From 19 to 27 March 2015, positive daily surface temperature anomalies were recorded throughout central and southern Chile (Figure 1). Highest daily surface temperature anomalies (generally  $+4^{\circ}\text{C}$  to  $+8^{\circ}\text{C}$ ) were seen in central Chile ( $30^{\circ}\text{S}$  to  $38^{\circ}\text{S}$ ; Figure 1) from 18 to 22 March 2015. Then, highest temperature anomalies (generally  $+8^{\circ}\text{C}$  to  $+11.5^{\circ}\text{C}$ ) were seen in south-central and southern Chile ( $38^{\circ}\text{S}$  to  $48^{\circ}\text{S}$ ) from 21 to 27 March. The absolute highest temperature anomaly ( $+11.2^{\circ}\text{C}$ ) was recorded in Valdivia ( $39.8^{\circ}\text{S}$ ,  $73.2^{\circ}\text{W}$ ) on 26 March. In the capital Santiago, at Pudahuel station (330021), an all-time record maximum temperature of  $36.8^{\circ}\text{C}$  was recorded on 20 March 2015 at 15:47 (local time), and at Quinta Normal (station 330020), an all-time record maximum temperature of  $36.2^{\circ}\text{C}$  was recorded on 20 March 2015 at 16:23 (local time).

Histograms of relative frequency of maximum daily 2 m air temperature (Figure 2) showed that the maximum daily 2 m air temperatures recorded throughout north-central, central, and south-central Chile, a region spanning more than  $20^{\circ}$  latitude, all fell at the extreme right end of the distributions for each city (Figure 2). At Santiago, the maximum air temperature at Pudahuel on 20 March 2015 was greater than any other recorded

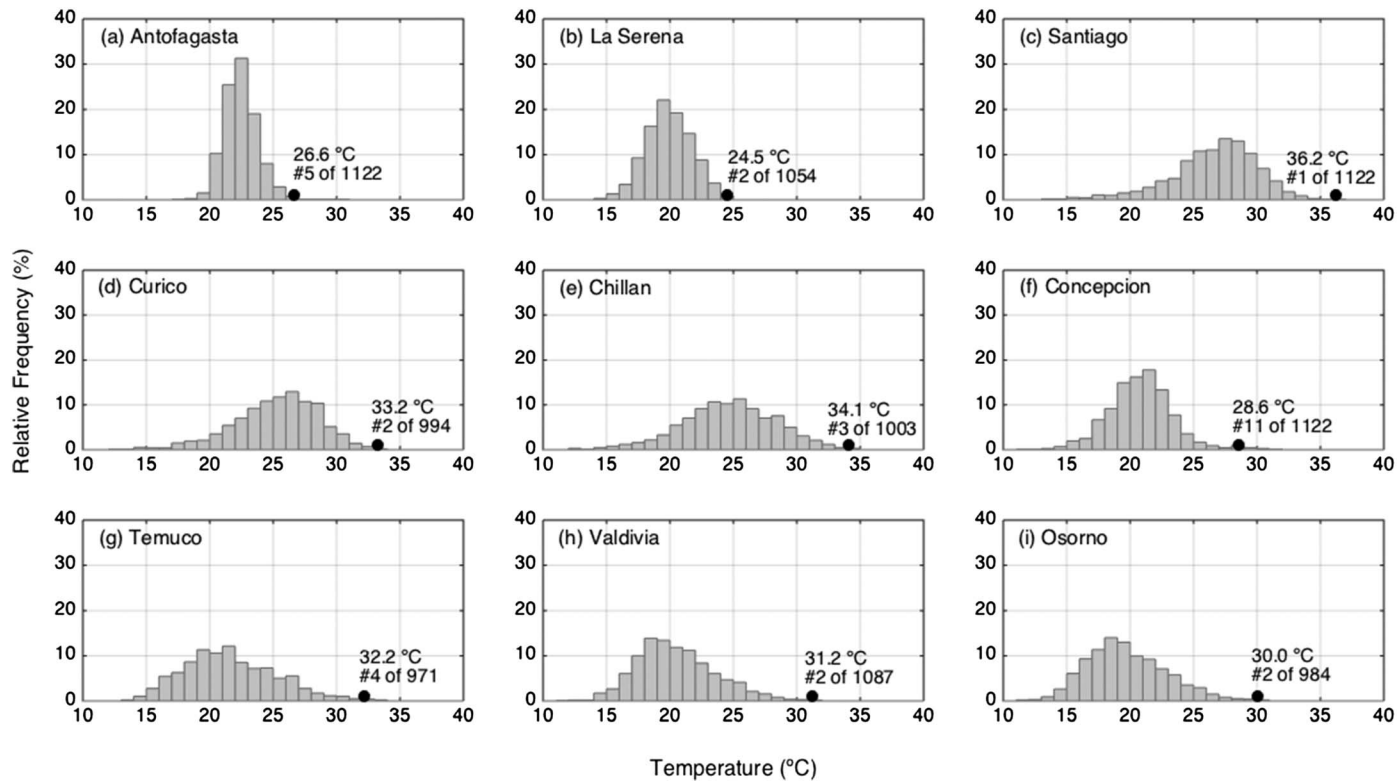


**Figure 2.** Histograms of relative frequency (in %; gray bars) of daily maximum surface air temperatures over the second half of March (15–30 March) from 1950 to 2015 (for La Serena, 1952–2015). Maximum surface air temperatures recorded at each station between 19 and 27 March 2015 reported as text and indicated by a black dot. Rank of each maximum temperature (and sample size  $n$ ) is reported also. Data from the Dirección de Meteorología de Chile (DMC).

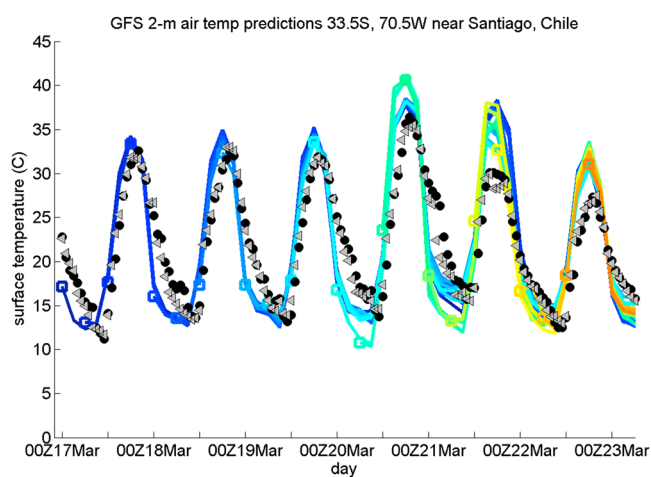


**Figure 3.** Predictions every 3 h of 2 m air temperature from the GFS model for 33.5°S, 70.5°W, the model location closest to (and including) the Santiago metropolitan region. Model simulations were initialized every 6 h beginning 0000 UTC 17 March 2015 and continuing through 1800 UTC 22 March 2015. Line color indicates initialization time (darker colors initialized earlier). Gray triangles indicate hourly temperature observed at Quinta Normal (station 330020), and black circles indicate temperature observed at Pudahuel (station 330021), both of which are in the central west portion of the metropolitan region.

in the history of the city (reliable records spanning back to 1877), and the observation ranked first out of 1122 observations for the second half of March (Figure 2c). At La Serena, Curicó, Valdivia, and Osorno (Figures 2b, 2d, 2h, and 2i, respectively), the observed maximum temperatures were the second highest in the 15–30 March historical record (of between 984 and 1087 observations). In Chillán (Figure 2e), the temperature was the third highest (of 1003 observations). It was the fourth highest (of 971 observations) in Temuco (Figure 2g), the fifth highest (of 1122 observations) in Antofagasta (Figure 2a), and the eleventh highest maximum temperature in the historical record (1122 observations) in Concepción (Figure 2f), confirming that the heat was a very rare event at all those stations.

To explore operational predictability of this extreme temperature event in Santiago, predictions of 2 m temperature

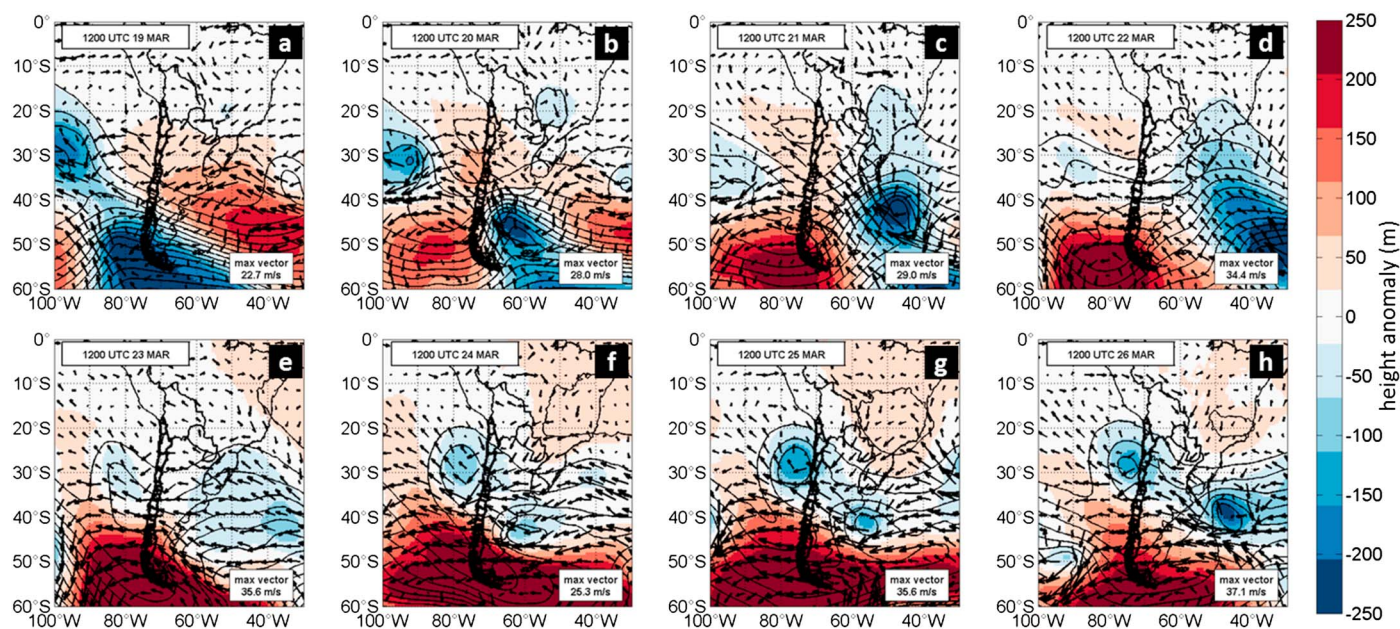


**Figure 4.** Analyses of 500 hPa height (black curves; in m), height anomalies (red and blue shading; in m), and wind anomalies (vectors), from GFS Final (FNL) analyses between (a) 1200 UTC 19 March 2015 and (h) 1200 UTC 26 March 2015. Anomalies determined by departure from March mean 1981–2010.

from the operational GFS model were examined for a 6 day period from 0000 UTC 17 March 2015 to 0000 UTC 23 March 2015 (Figure 3). Observed temperatures at both Quinta Normal (330020; 33.45°S 70.68°W, 510 m above sea level) and Pudahuel (330021; 33.37°S 70.77°W, 476 m above sea level) showed that the record temperatures observed on 20 March 2015 were predicted by the GFS with a lead time of as much as 4 days (Figure 3). Indeed, predictions from the GFS simulations initialized at 0000 UTC 20 March and 0600 UTC 20 March both overpredicted temperatures by nearly 4°C (green curves Figure 3). However, that overprediction could be due to the horizontal resolution of the GFS model, as the grid box that includes Santiago (with a diameter of approximately 40 km at the latitude of Santiago) spans nearly the entire central valley and includes both Pudahuel and Quinta Normal. Predictions from GFS simulations initialized on 18 and 19 March (dark blue and cyan curves, Figure 3) best predicted the extreme maximum surface air temperatures. None of the GFS simulations examined for this study accurately predicted the cooler maximum temperatures observed on 21 and 22 March (black circles and grey triangles, Figure 3), instead indicating a continuation of the heat event through 22 March 2015.

To better understand the physical mechanisms behind the high surface temperatures recorded in central Chile, synoptic charts of different variables and their anomalies (i.e., height, wind, sea level pressure, and temperature) were examined at different levels (500 hPa, surface, and 850 hPa) for the period 19 March 2015 to 26 March 2015. This period was selected to encompass both the extreme temperature event in central Chile of 19–21 March 2015, the extreme precipitation event in northern Chile of 22–25 March 2015, and the extreme heat event in south-central and southern Chile of 22–26 March 2015. The precipitation event is explored in more detail in the next section. At 500 hPa (Figure 4), on 19 March, weak anomalous ridging (+50 m heights) was seen over central Chile, extending to stronger anomalous ridging (+200 m) east of Argentina (Figure 4a). A deep anomalous trough (height anomalies of  $-250$  m) was centered west of southern Chile. The northwestern extent of the anomalous ridge-trough axis terminated in a cutoff, closed low (height anomaly of  $-150$  m) near 30°S, 100°W. This cutoff low slowly progressed east (translating eastward at approximately  $2.5 \text{ m s}^{-1}$ ) and later served as a catalyst for the heavy precipitation event. This anomalous trough-ridge pattern was identified by *Ruttlant and Garreaud* [2004] as typical during approximately 20% of “Raco” wind (warm easterly downslope winds) episodes: the 500 hPa height pattern in their Figure 6b compares very favorably with the 500 hPa height field seen in our Figure 4a at 1200 UTC 19 March. This similarity in height fields is notable despite the seasonal difference (*Ruttlant and Garreaud* [2004] studied winter, and this was a late summer event that featured anomalous troughing and ridging more typical of winter). This synoptic-scale pattern

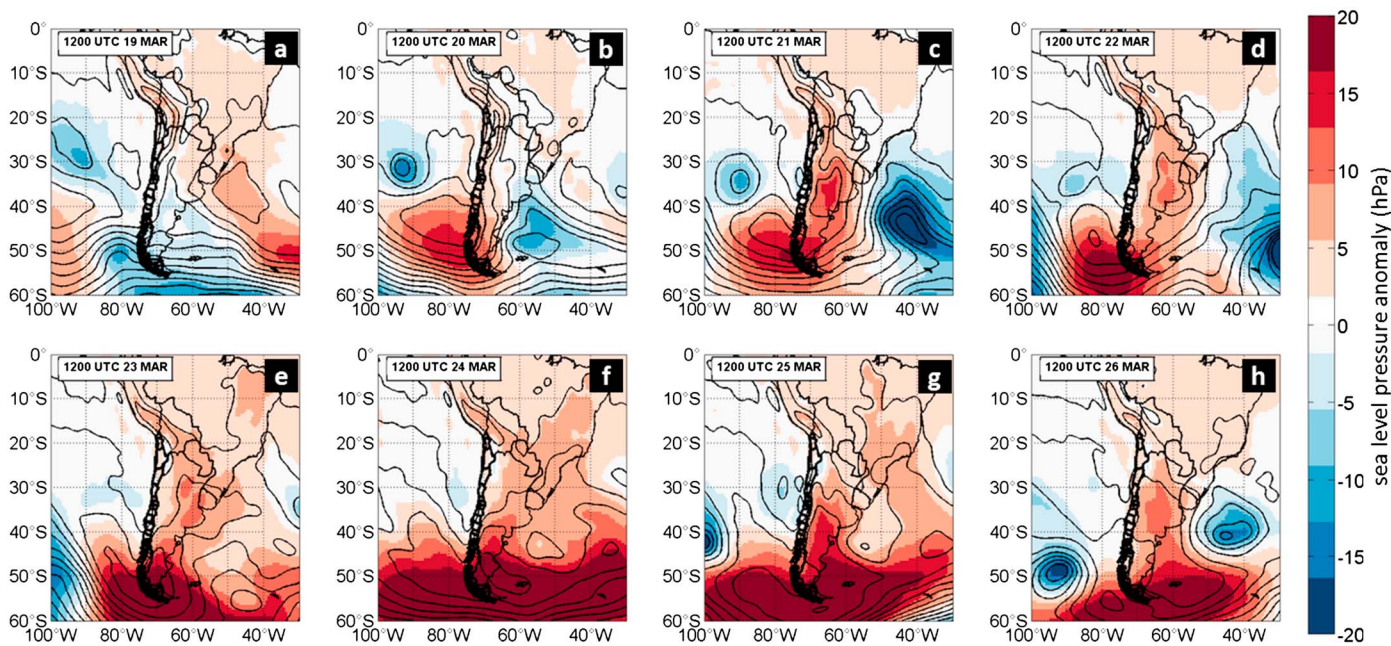


**Figure 5.** As in Figure 4 but for sea level pressure (black curves) and anomalies (shading), in hectopascal from GFS FNL analyses.

on 19 March 2015, favoring warm air atop a cool stable boundary layer, served as a precursor to the record temperature event of 20 March 2015 in the Santiago metropolitan area. On 20 March 2015, 500 hPa heights were characterized by a wave train extending across southern South America with a ridge west of Chile near 50°S, 85°W, a trough over eastern Argentina near 45°S, 60°W, and another ridge in the South Atlantic near 50°S, 40°W (Figure 4b). In the subtropics, an anomalous ridge (+50 to +100 m height anomalies) extended down the coast of northern Chile to a maximum centered nearly over Santiago (Figures 4b and 4c). This ridge weakened and shifted slowly north after the extreme temperature event, and by 22 March 2015 (Figure 4d), neutral 500 hPa heights were found over central Chile. By 23 March 2015 (Figure 4e), height anomalies at 500 hPa turned negative over central Chile and strongly positive (+300 m anomaly) over southern Chile and the straits between Chile and Antarctica. That pattern of negative height anomalies over central Chile and strongly positive height anomalies over southern Chile continued through 26 March 2015 (Figure 4h).

Sea level pressures and anomalies during this 8-day period resembled 500-hPa height field and anomalies (Figure 5). For example, at 1200 UTC on 19 March 2015, two surface troughs were identified, one west of southern Chile extending NNW to a surface low near 30°S, 90°W (with spherical Langmuir probe (SLP) anomalies approaching  $-10 \text{ hPa}$ ) and another over western Argentina in the lee of the Andes (SLP anomalies approaching  $-5 \text{ hPa}$ ) (Figure 5a). Over central and northern Chile, subtle surface ridging (anomalies up to  $+5 \text{ hPa}$ ) was seen. By 20 March 2015, surface ridging was seen over southern Chile (SLP anomalies up to  $+15 \text{ hPa}$ ), and subtle surface troughing (anomalies up to  $-2 \text{ hPa}$ ) was seen along the coast of central and northern Chile, with ridging still seen over the northern Chilean Andes and the Bolivian Altiplano (Figure 5b). The coastal trough amplified by 21 March 2015, the day after the highest temperatures were recorded, with SLP anomalies of  $-5 \text{ hPa}$  seen centered near 35°S (Figure 5c). For the next 5 days, sea level pressures continued with a pattern of coastal troughing, and on 25 March 2015 (Figure 5g), the coastal trough was seen to have merged with the cutoff low that slowly approached from the west. Along with the approach of the cutoff low, SLP anomalies in southern Chile and the strait between South America and Antarctica increased, peaking on 24 March 2015 (Figure 5f) nearly  $+30 \text{ hPa}$  above March monthly normal.

At 850 hPa, temperature and circulation anomalies at the start of the period at 1200 UTC 19 March 2015 showed above normal temperatures ( $+2^\circ\text{C}$  to  $+5^\circ\text{C}$ ) extending from central Chile eastward into the southwest South Atlantic (Figure 6), roughly colocated with the anomalous ridge at 500 hPa. Circulation at 850 hPa over central Chile was southeasterly. On both 20 and 21 March 2015, anomalous 850 hPa temperatures of  $+8^\circ\text{C}$  were seen over central and south-central Chile, together with easterly and southeasterly anticyclonic flow

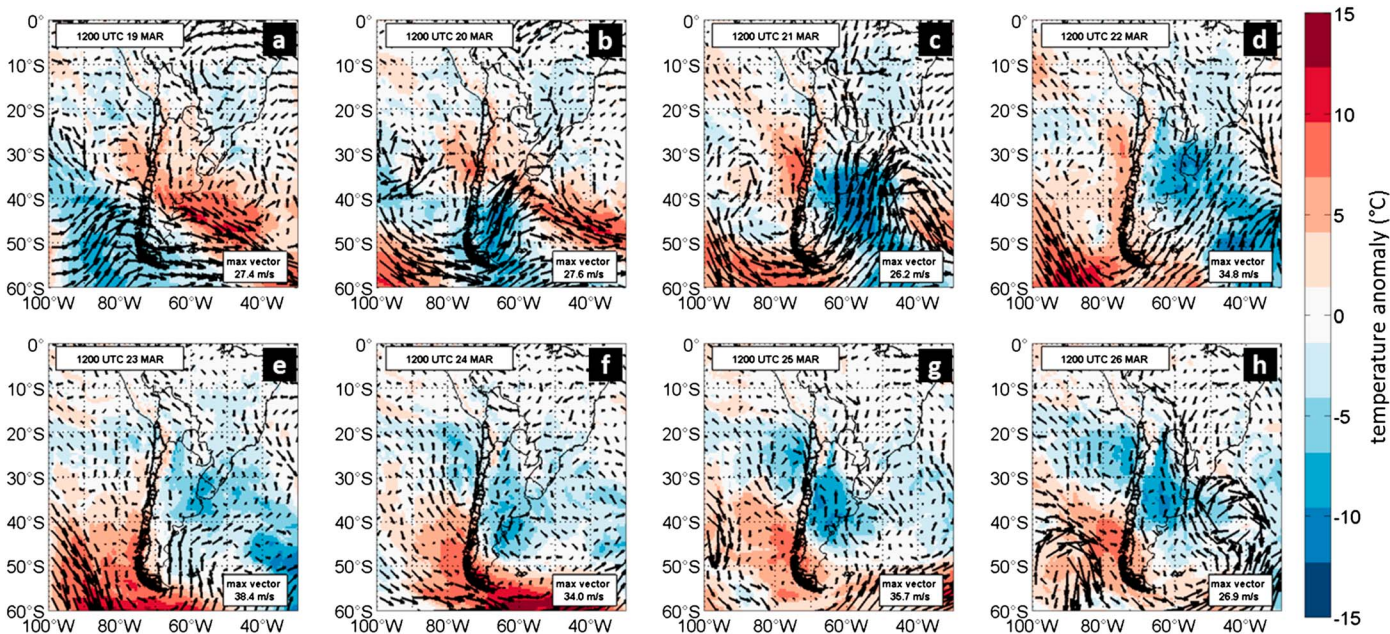


**Figure 6.** As in Figure 4 but for 850-hPa temperature anomalies (shaded; in °C) and actual winds (vectors) from GFS FNL analyses.

immediately along the coast. The larger-scale flow at 850 hPa on both days was mostly anticyclonic south of 40°S and cyclonic north of 40°S (Figures 6b and 6c). The largest expanse of positive 850 hPa temperature anomalies (over +5°C extending north from 40°S along the Chilean coast to about 25°S 75°W) was seen at 1200 UTC on 21 March 2015 (Figure 6b), the day after the highest surface temperatures were seen. In general, anomalous 850 hPa temperatures over much of the southern half of South America in Figures 6e–6g were colocated with the similarly signed 500 hPa height anomalies (Figures 4e–4g). Thus, as the 500 hPa circulation anomaly shifted away from ridging and toward troughing over central and northern Chile (Figures 4e–4h), the 850 hPa temperature anomalies also changed signs, with weak (+1°C to +2°C) positive anomalies on 23 March 2015 (Figure 6e) turning negative (−1°C to −2°C) by 24 March 2015 (Figure 6f) and staying negative through 26 March 2015 (Figure 6h).

The vertical structure of temperature at 1200 UTC (0800 local time) at four stations (Antofagasta, Santo Domingo, Puerto Montt, and Punta Arenas) over the 19–26 March 2015 period also showed variability (Figure 7). At Santo Domingo, the only regular sounding station in central Chile, a temperature inversion was seen on both 20 to 21 March 2015, with maximum temperatures in the inversion peaking near 27°C around 915 hPa on 20 March 2015, coinciding with the day of highest maximum temperatures. By 22 March 2015, the temperature inversion at Santo Domingo had substantially eroded. This temperature pattern evolution is consistent with work by *Ruttlant and Garreaud* [2004] during easterly “Raco” downslope wind events. For example, between 19 and 21 March 2015, 850 hPa observed wind directions on the Santo Domingo radiosonde were between 145° and 160° (southeasterly), with speeds increasing from  $5 \text{ m s}^{-1}$  on 19 March 2015 to  $12 \text{ m s}^{-1}$  on 20 March 2015. This easterly component flow is in accordance with the minimum in sea level pressure along the coast (Figure 5c), and the southeasterly low-level jet is consistent with a “Raco” wind event favoring increased subsidence and warming in the interior valleys of central Chile. Along with the transition to coastal troughing (Figure 5) and northerly near-surface winds (Figure 6) in the subsequent 5 days, the troposphere also moistened at Santo Domingo between 21 and 25 March. During that period, dew point temperatures above the inversion increased from near  $-20^\circ\text{C}$  on 19 March 2015 to  $+10^\circ\text{C}$  on 25 March 2015. At Puerto Montt (41.5°S, 72.9°W), temperatures just above the boundary layer (near 975 hPa) increased from around 5°C on 19 March 2015 to above 20°C on 25 March 2015. This increase in temperature coincided with the onset of strong positive anomalies in maximum surface temperature recorded across south-central and southern Chile and agrees with *Bumbaco et al.* [2013] who found similar temperature anomalies over the areas west of the Cascade Mountains (a region with a climate similar to southern

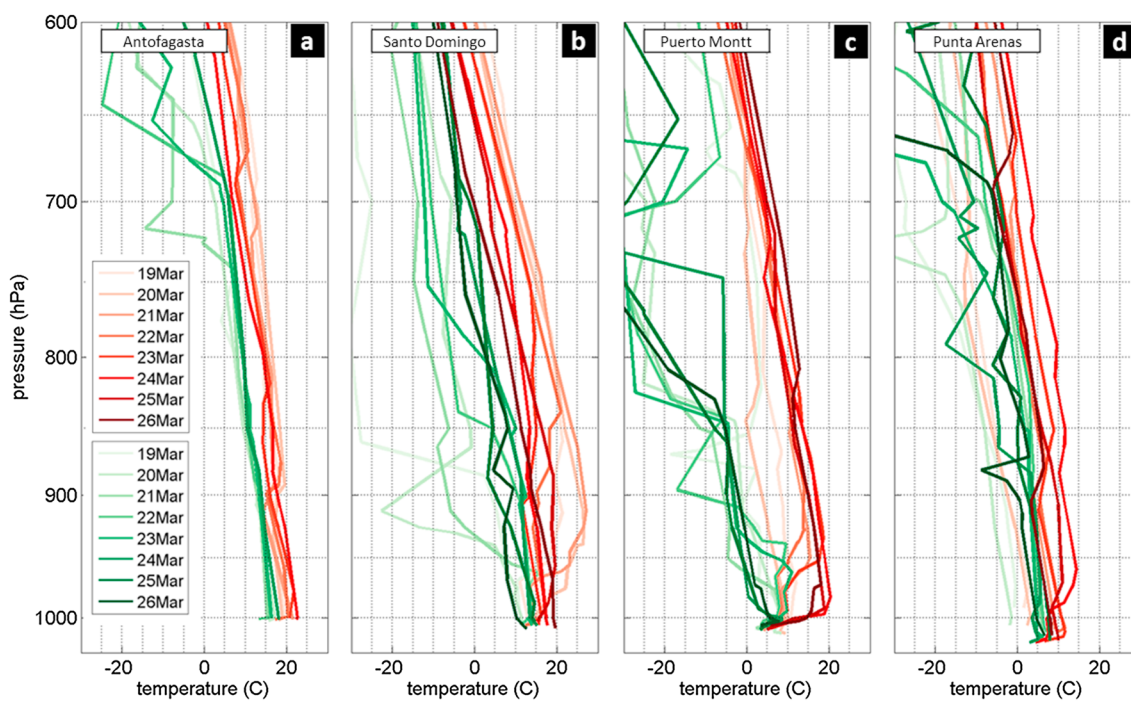


**Figure 7.** Upper air observations of air temperature (red-orange curves; in °C) and dew point temperature (green curves; in °C) from (a) Antofagasta, (b) Santo Domingo, (c) Puerto Montt, and (d) Punta Arenas from 19 to 26 March 2015. Lighter curves indicate earlier observations. Antofagasta observations only available from 19 to 24 March 2015. Station locations are indicated by purple dots in Figure 1. All data are from NOAA Integrated Global Radiosonde Archive (IGRA).

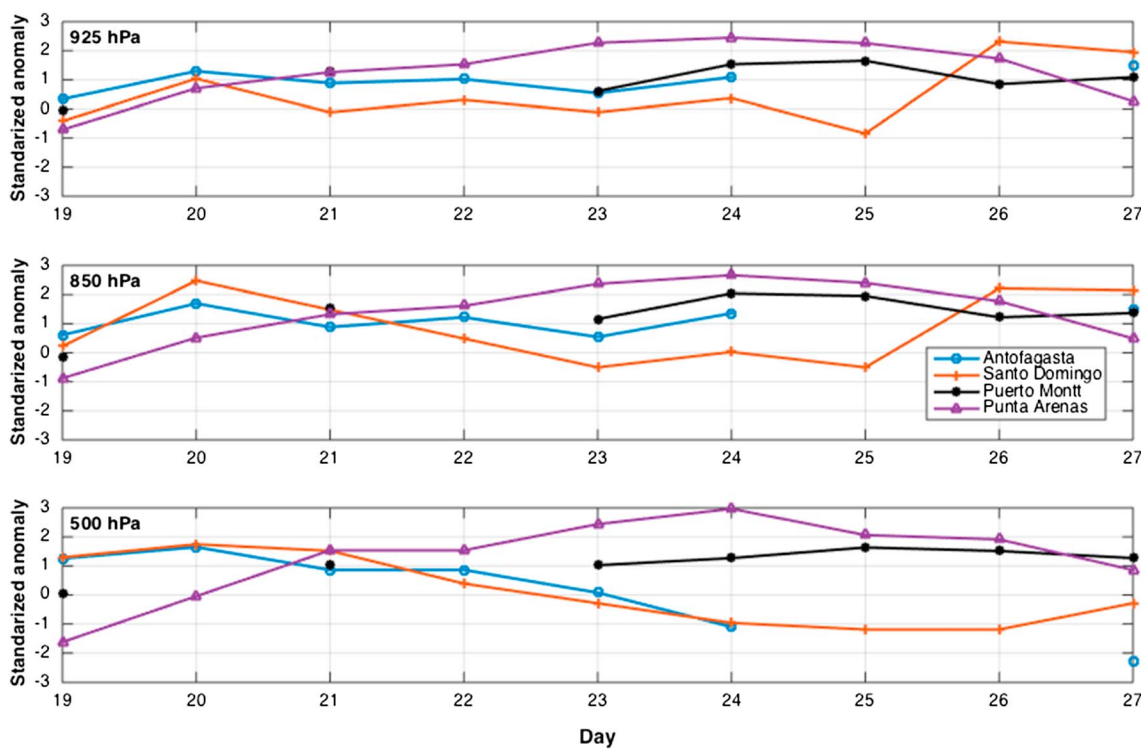


**Figure 8.** Standard anomalies of March upper air height from 19 to 27 March 2015 (anomalies based on 1994–2015 mean) at 925, 850, and 500 hPa from the 1200 UTC (0900 local) upper air observations at the four radiosonde sites with temperatures analyzed in Figure 7 (site locations indicated on Figure 1b). Gaps in lines indicate days in which upper air data were not available at that pressure level. All data are from NOAA Integrated Global Radiosonde Archive (IGRA).

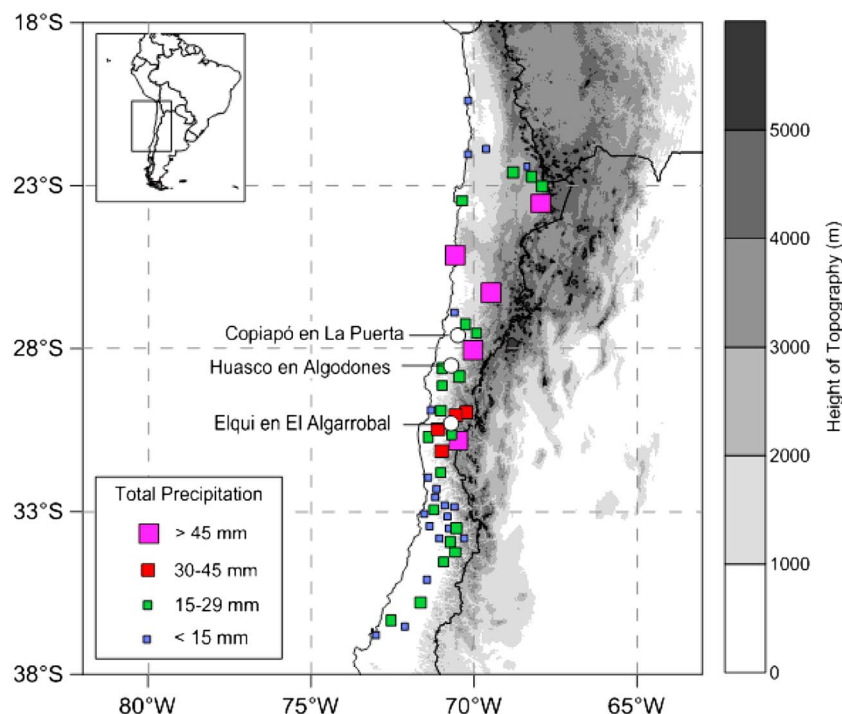


**Figure 9.** Accumulated precipitation (black squares; size indicates precipitation total in mm) from 23 to 27 March 2015. Maximum precipitation recorded was 87 mm at El Salvador station ( $26.2^{\circ}\text{S}$ ,  $69.6^{\circ}\text{W}$ , elevation 2260 m). Labeled white circles indicate locations of streamflow observation stations in Figure 12. Data are from the Chilean Dirección Meteorológica and Dirección de Aguas.

Chile). Boundary layer drying was also noted leading up to the heat event, as dew point temperatures at 950 hPa decreased from near  $10^{\circ}\text{C}$  on 19 March 2015 to  $0^{\circ}\text{C}$  on 25 March 2015. At Punta Arenas ( $53.2^{\circ}\text{S}$ ,  $70.9^{\circ}\text{W}$ ), temperatures throughout the lower and middle troposphere (extending up to 400 hPa) warmed nearly  $10^{\circ}\text{C}$  between 19 and 26 March 2015. This warming is very consistent with the development of the pronounced, expansive, and anomalously strong upper ridge and surface high pressure seen in Figures 4 and 5.

Although the highest surface air temperatures were recorded in central Chile, the largest low and middle troposphere height anomalies were observed in southern Chile. This anomaly pattern was confirmed in analysis of heights at 925, 850, and 500 hPa at the four radiosonde upper air sites in Chile (Figure 8). Between 23 and 25 March, Punta Arenas recorded anomalies over 2 standard deviations above normal in the lower and middle troposphere (anomalies were based on the Punta Arenas radiosonde record from 1994 to 2015). The observed 500 hPa height observed at 1200 UTC on 24 March 2015, 5820 m, was the highest since upper air observations began there in 1994. Heights at 925, 850, and 500 hPa exceeded the 99th percentile of March values. These record heights confirmed the presence of a strong, deep blocking anticyclone whose circulation advected the cutoff eastward into northern Chile. At Puerto Montt (500 km to the north of Punta Arenas), similarly anomalous positive heights were seen, although not as strong as at Punta Arenas, indicating the confinement of the blocking high to the south and the closer proximity to the cutoff low. At Santo Domingo, 850 hPa height anomalies were more than 2 standard deviations above normal on 20 March 2015, anomalies that were seen on the day of the record warmth in Santiago. Finally, in northern Chile at Antofagasta, 500 hPa heights were 1 standard deviation below normal at 1200 UTC on 24 March 2015. This observation indicates that the height depression of the cutoff low was anomalous, but not extremely so, only around one standard deviation below normal. Interestingly, 925 hPa and 850 hPa heights at Antofagasta on 24 March were approximately 1 standard deviation above normal, indicating the presence of warm air in the lower troposphere that contributed to instability just before the onset of the period of heaviest precipitation. (upper air observations at Antofagasta were unavailable from 25 to 27 March 2015).

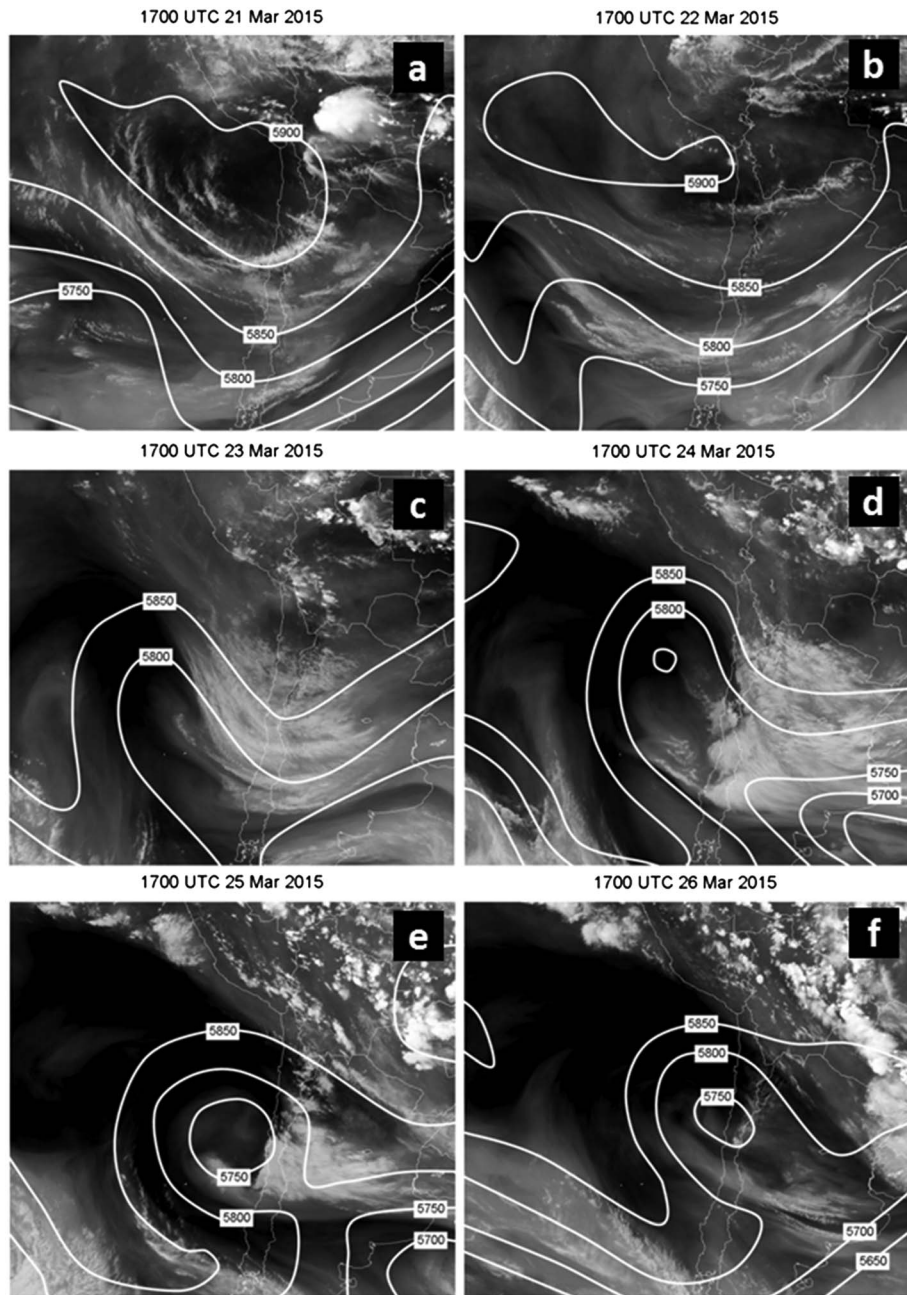


**Figure 10.** Infrared satellite images from GOES East (GOES 13), daily at 1700 UTC (1400 Local), from (a) 21 March 2015 to (f) 26 March 2015. White curves indicate 500 hPa height (in m) from GFS analyses.

To summarize, the presence of the blocking anticyclone to the south effectively reversed the mean climatological latitudinal height and pressure gradient along the Chilean coast. This reversal of the climatological mean surface pressure gradient (Figure 5) created an easterly wind component in the lower to middle troposphere in central Chile as seen in Figures 6a–6c, which was especially evident during 20 and 21 March. The peak anomalous zonal winds of  $-3.2 \text{ m s}^{-1}$  at 1200 UTC on 20 March 2015 were in the 98th percentile for zonal winds at 850 hPa in March from 1988 to 2015, implying that only 2% of March observations in the 28 years prior to this event had stronger zonal wind components. Given the presence of the Andes, 850 hPa winds with an easterly component produce strong descent and clear sky conditions that favor the formation of surface troughing or the development of coastally trapped lows [Garreaud et al., 2002]. Given

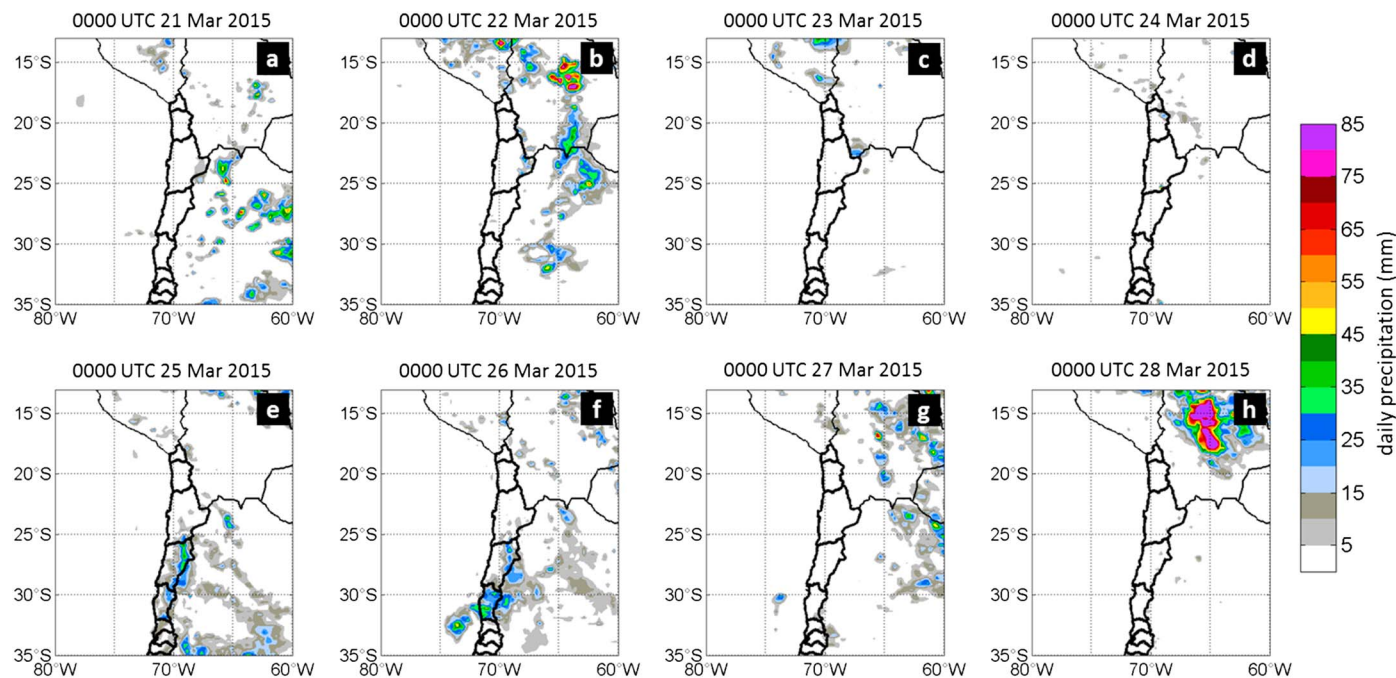


**Figure 11.** Accumulated precipitation from Tropical Rainfall Measuring Mission (TRMM) 3B42 version 7 satellite observations (in mm) for 24 h periods ending at (a) 0000 UTC 21 March 2015 (2100 local time 20 March 2015) to (h) 0000 UTC 28 March 2015.

the already demonstrated connection between the southern migrating anticyclones and the development of easterly component winds in central Chile with compensating subsidence, it is reasonable to hypothesize that the extremeness of the high associated with this event produced an extreme realization of the coastal low mechanism. These types of coastal lows are a relatively common occurrence during the passage of strong migrating anticyclones and baroclinic activity in southern Chile [Garreaud *et al.*, 2002]. In typical coastal low events, the surface circulation may still be from the west and therefore act to ventilate air from the marine boundary layer into the central valleys, including into Santiago. However, given that the timing of this particular coastal low event coincided with the climatological annual maximum in sea surface temperatures along the central Chilean coast, the reduction of near-surface air temperatures by mixing of the maritime air advected inland was less effective, thus contributing to the extreme heat event. Additional influences from other modes of atmospheric variability, including the intraseasonal through the decadal, also potentially influenced this event, and future work may consider their roles.

### 3.2. Extreme Precipitation

From 19 to 26 March 2015, northern Chile experienced an unusual and extreme rainfall event. Unlike nearly all precipitation events in Chile, maximum rainfall was located equatorward of 32°S (for example, El Salvador station, 26.2°S, 69.6°W at 2240 m elevation, recorded 87.0 mm, the maximum observed during this event) (Figure 9). Indeed, in central Chile from 32°S to 38°S, most stations recorded fewer than 15 mm, while in north-central Chile from 29°S to 32°S, mean station precipitation was between 15 and 45 mm. North of 29°S, several stations recorded greater than 45 mm. The primary forcing for this precipitation event came from an eastward moving cutoff low. This cutoff low was seen in height anomalies at 500 hPa ( $-200$  m) and pressure anomalies at sea level ( $-10$  hPa) as early as 19 March 2015, centered near 30°S, 100°W (Figures 4 and 5). By 22 March 2015, both the 500 hPa height anomalies and sea level pressure anomalies had diminished, indicating that the low had weakened. However, this weakening was temporary, and by 24 and 25 March 2015, 500 hPa heights were again as low as 100 m below normal, and sea level pressures were 5 hPa below normal. By 26 March, the closed low had arrived at the coast and was centered near 25°S (Figure 4h). From 20 to 23 March, in the days leading up to the heavy precipitation event, scattered convective precipitation was seen in the Peruvian and Bolivian Altiplanos, over the Chilean Andes, and east in the plains of Argentina (Figures 10a and 10b and 11a–11d). The 24 h period ending 1200 UTC 24 March 2015 saw substantial precipitation (over

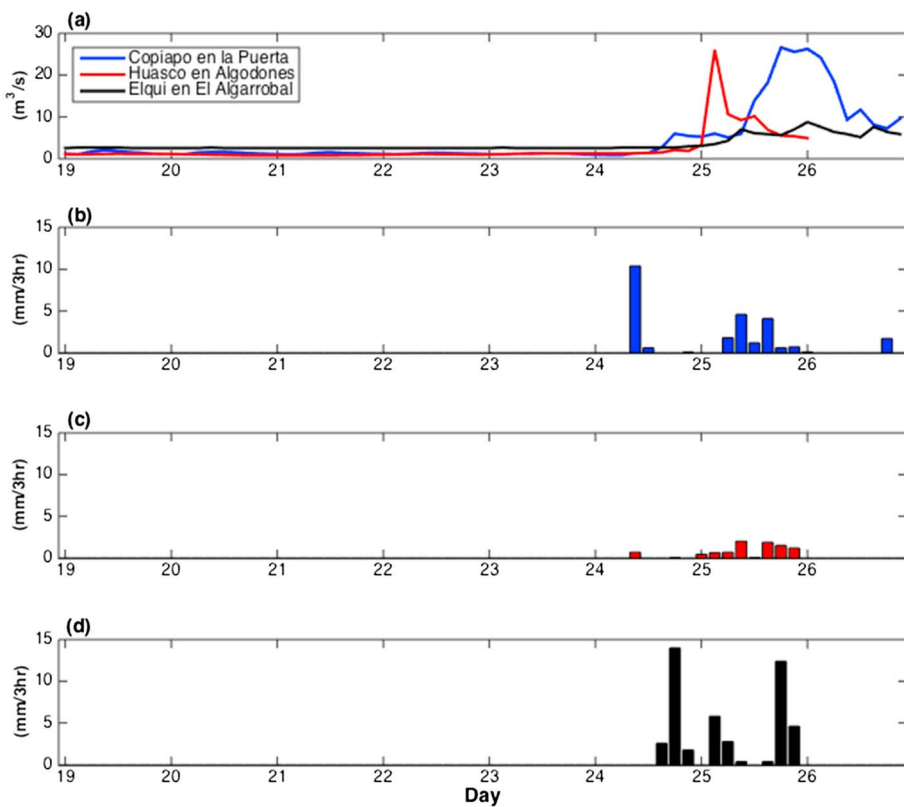


**Figure 12.** (top) Streamflow (in  $\text{m}^3 \text{s}^{-1}$ ) and (bottom) accumulated precipitation (in  $\text{mm} (3 \text{ h})^{-1}$ ) at three stations in northern Chile. Stations ordered from north to south and indicated by white dots in Figure 9. Data are from the Chilean Dirección de Aguas.

85 mm) over the central Chilean Andes (Figure 11e), indicative of the approach of the cutoff low and reduction in static stability. The heavy precipitation event itself began in the afternoon of 24 March (seen as cold cloud tops in infrared imagery; Figure 10d) and lasted through 27 March (Figures 11f–11h). Heaviest precipitation over the Atacama was centered between  $24^\circ\text{S}$  and  $28^\circ\text{S}$  on 24 and 25 March. The spatial and temporal distribution of precipitation totals from TRMM observations agreed qualitatively with gauge observations: maximum TRMM observations were seen from  $23^\circ$  to  $30^\circ\text{S}$  on 24 and 25 March 2015 (Figures 11e and 11f), similar to gauge observations. Streamflow measurements in the heart of the region of heaviest precipitation indicated flow rates, sometimes extreme, that lagged precipitation by several hours (Figure 12). Three stations analyzed for this study, Copiapó, Huasco, and Elqui (positions labeled in Figure 9), featured baseline flow rates of less than  $2 \text{ m}^3 \text{s}^{-1}$  (Figure 12a). At Copiapó, 10 mm of precipitation was observed around midday 24 March 2015, followed by another 20 mm of precipitation on 25 March (Figure 12b). By the end of the day on 25 March, volumetric flow rates at Copiapó approached  $30 \text{ m}^3 \text{s}^{-1}$ . Volumetric flow at Huasco spiked to similar rates on 25 March, although because of the high rainfall and streamflow, Huasco station stopped reporting on at 2300 UTC (1900 local) 25 March 2015 (Figure 12a), making it more difficult to determine if high streamflow rates there were the result of upstream precipitation collecting and flowing into the catchment or if it was the result of in situ precipitation. The farthest south station, Elqui, had lower flow rates and fewer spikes, this despite several periods of 3 h rain rates approaching  $10 \text{ mm} (3 \text{ h})^{-1}$  (Figure 12d), and this agreed with the civil protection service reports of strongest and most damaging mudflows in the northern stations.

The primary forcing for this heavy precipitation event came from the approach of an upper troposphere cutoff low. However, as noted by Garreaud and Fuenzalida [2007], cutoff lows in March do not always produce precipitation in the Atacama. The northward position of the cutoff low contributed to the northward expansion of precipitation, although the 500 hPa height anomaly at Antofagasta on 24 March 2015 was only

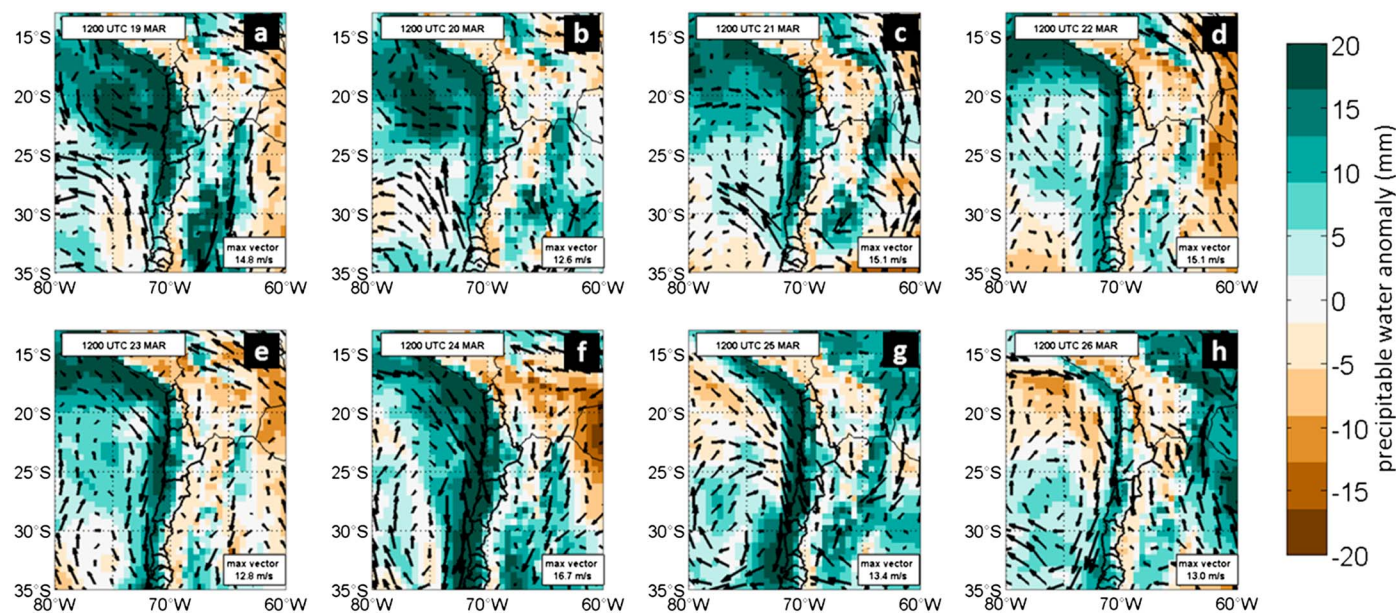


**Figure 13.** As in Figure 4 but for precipitable water content anomalies (in mm) and 850 hPa winds (in  $\text{m s}^{-1}$ ) from GFS FNL analyses. Anomalies of precipitable water are with respect to 1981–2010 March mean.

1 standard deviation below normal (Figure 8). Another likely contributor to both the northern location and the heavy nature of the precipitation was the very high precipitable water anomalies observed over the Peruvian bight and adjacent coastal zones (Figure 13). Precipitable water anomalies approaching 20 mm above normal were seen throughout the 8 day period leading up to the heavy rainfall event. Starting on 22 March 2015 (Figure 13d), 850 hPa winds adjacent to the coast became northerly ahead of the approaching cutoff low (wind speeds as much as  $4 \text{ m s}^{-1}$  above normal). These northerly winds advected high precipitable water content air onto the Atacama. They also advected warmer than normal air in the lower troposphere, seen as an increase in lower troposphere temperatures in the Antofagasta sounding (Figures 7 and 8). Accordingly, positive values of Convective Available Potential Energy (CAPE) were recorded for surface parcels from the 1200 UTC 24 March 2015 Antofagasta sounding, and relatively higher values of CAPE were recorded for parcels with origin above

700 hPa (not shown). These high precipitable water values and surface and mid-troposphere instability then enhanced convective precipitation rates once the cutoff low reached the coast. By 1200 UTC 26 March (Figure 13h), toward the conclusion of the heavy rain event, precipitable water anomalies had fallen back to near +5 mm over the immediate coastal zone. The high precipitable water values were likely the result of anomalously warm sea surface temperatures (SSTs) off the coast of Perú, as much as  $3^{\circ}\text{C}$  above 1981–2010 climatological March normal values (Figure 14). These warmer than normal SSTs were potentially a consequence of the warming of the eastern equatorial Pacific Ocean during the 2015 El Niño event [Bell et al., 2015], although it is notable that anomalies in the Niño 1.2 region jumped

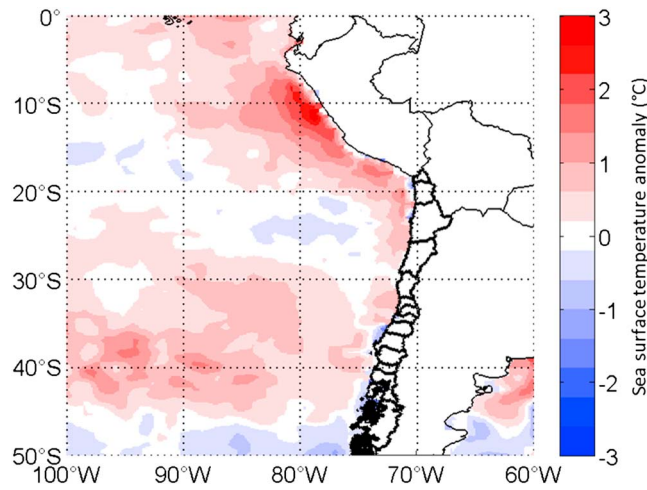


**Figure 14.** Sea surface temperature anomalies (in  $^{\circ}\text{C}$ ) for 20–24 March 2015. Sea surface temperature values averaged from ERA Interim 6 h analyses across the 5 day period and calculated from March 1981–2010 climatological norms.

from  $-0.5^{\circ}\text{C}$  on 04 March 2015 to  $+1.2^{\circ}\text{C}$  on 25 March 2015, a difference of  $1.7^{\circ}\text{C}$  in only 3 weeks. This difference suggests those SST changes may have occurred on a faster time scale than El Niño alone.

#### 4. Discussion and Conclusions

An extreme precipitation event in northern Chile occurred immediately after an extreme heat event in central Chile and concurrent with an extreme heat event in south-central and southern Chile. Evolution of 500 hPa height and wind fields, 850 hPa temperature and wind fields, and SLP fields suggested that the events occurred during an amplified and blocked flow pattern. For example, while height anomalies at 500 hPa over central and northern Chile switched signs over the week-long period (providing evidence against flow blocking at the northern latitudes), a pronounced ridge at 500 hPa (centered near  $100^{\circ}\text{W}$  on 19 March 2015) moved eastward, and by 20 March 2015, the axis was located near  $80^{\circ}\text{W}$ , evidence for flow blocking in the southern latitudes. By 26 March 2015, the ridge axis was centered near  $90^{\circ}\text{W}$ , and the 500 hPa height anomalies—only 100 m above normal on 20 March—grew in both spatial extent and amplitude (300+ m above normal) through 26 March 2015. This expansive and strong upper level ridge provided at least three important physical forcing mechanisms for the extreme temperature and precipitation events of the week. First, as it approached Chile from 19 to 20 March 2015, the upper level ridge acted to reverse the climatological latitudinal surface pressure gradient and thereby produced anomalous easterly flow and subsidence, leading to strong insolation and warm boundary layer conditions that produced the extreme heat in central Chile. Indeed, at Santo Domingo, maximum easterly 850 hPa wind anomaly ( $-3.2 \text{ m s}^{-1}$ , in the 98th percentile of March observations from 1988 to 2015) was observed at 1200 UTC on 20 March 2015, and easterly 850 hPa wind anomalies at Santo Domingo began on 15 March 2015. Second, by amplifying and expanding from 21 to 26 March 2015, circulation associated with the upper level ridge acted to advect anomalous potential vorticity along its leading western edge, promoting the formation and strengthening of the upper level low to its north. As shown by Renwick and Revell [1999], atmospheric blocking anticyclones, such as the one present during March 2015, are associated with cyclonic anomalies downstream over Southern South America, which composites show also as negative anomalies of vorticity over central Chile resembling the northeast to southwest tilt of the precursor of the cutoff low. By the date of the landfall of the cutoff low in northern Chile (25 March 2015), height anomalies over 200 m above normal extended along  $60^{\circ}\text{S}$  from  $110^{\circ}\text{W}$  to  $30^{\circ}\text{W}$ , nearly a 5000 km expanse. This type of high-over-low tropospheric height pattern was identified by Rex [1950] as a classic atmospheric blocking pattern. Third, this southern blocking ridge [e.g., Trenberth and Mo, 1985; Marques and Rao, 1999; Damião Mendes and Albuquerque Cavalcanti, 2014] provided subsidence and insolation needed for the strong positive surface temperature anomalies observed in south-central and southern Chile at the end of the 1 week period. Perhaps because of the established synoptic forcing for the heat event, global model predictions (from the GFS) captured the potential for record-setting heat as much as 4 days before it occurred. As such, one operational implication from this event is for forecasters to realize the current capabilities of large-scale models to accurately predict this type of extreme event.

Although circulation around the strong midtroposphere ridge seen over southern Chile aided in advecting the cutoff upper low mostly eastward during its approach to the coast, it is important to recognize that other conditions, besides forcing from the cutoff low itself, were also instrumental in producing the heavy rains and resulting catastrophic streamflow. Indeed, Garreaud and Fuenzalida [2007] discussed a cutoff low from March 2005 that drifted eastward and came ashore in central Chile (near  $30^{\circ}\text{S}$ ) but without extreme precipitation. Perhaps the most important contributing factor in this 2015 case, and one different from the March 2005 case, was the presence of anomalous above normal precipitable water equatorward of the upper level low. On 19 March 2015, the entire Peruvian bight region featured atmospheric precipitable water (PW) values 15–20 mm above normal. The circulation around the cutoff low advected this moisture southward, parallel to the coast. By 24 March 2015, precipitable water anomalies of +20 mm were seen along the entire Chilean coast from Arica ( $18^{\circ}\text{S}$ ) south to  $35^{\circ}\text{S}$ . Anomalies on the eastern side of the Andes were near zero, or even negative, suggesting that all of this moisture was trapped against the cordillera. Convective precipitation developed in the unstable conditions characteristic of the leading part of the upper level low and tapped this anomalous PW, leading to the extreme precipitation and very high streamflows observed in the Atacama. Once the cutoff low moved into Argentina, negative PW anomalies were seen in the Peruvian bight region. The connection between the atmospheric PW anomaly and the sea surface temperature anomaly over the coast of Perú was shown to be related to the precipitation over the hyperarid region

(D. Bozkurt et al., Impact of warmer eastern tropical Pacific SST on the March 2015 Atacama floods, submitted to *Monthly Weather Review*, 2016). Because of the synoptic-scale conditions preceding this heavy precipitation event, operationally, forecasters facing the possibility of a similar extreme precipitation event could take into account precipitable water anomalies and predicted boundary layer wind trajectories. They should also be aware that it does not take an extreme cutoff low to produce extreme precipitation, evidenced by 500 hPa height anomalies at Antofagasta reaching only one standard deviation below normal at 1200 UTC 24 March 2015. Forecasters could take into account tropospheric blocking over central and southern Chile as a precursor to forcing the eventual trajectory of a cutoff upper low. Anecdotal reports from northern Chile after the extreme flooding suggest lack of awareness of the potential severity of this event. Furthermore, it is possible that other atmospheric phenomena operating on larger spatial and temporal scales, including the El Niño–Southern Oscillation, the Madden-Julian Oscillation, and the Southern Annular Mode, contributed to the evolution of the synoptic-scale patterns observed during this event, and future work could focus on those influences.

#### Acknowledgments

The authors would like to thank the anonymous reviewers for their helpful comments and feedback. The collaborative idea for this study was inspired by travel funded by the International Programs Office of the U.S. Naval Academy. R.R. acknowledges support from FONDAP Research Center (CR)2 (15110009). All data for this paper is properly cited and referred to in the manuscript and reference list.

#### References

- Barrett, B. S., R. D. Garreaud, and M. Falvey (2009), Effect of the Andes Cordillera on precipitation from a midlatitude cold front, *Mon. Weather Rev.*, 137(9), 3092–3109, doi:10.1175/2009MWR2881.1.
- Bell, G. D., W. Shi, M. L'Heureux, and M. Halpert (2015), Climate diagnostics bulletin. [Available at [http://www.cpc.ncep.noaa.gov/products/CDB/CDB\\_Archive\\_html/bulletin\\_032015/](http://www.cpc.ncep.noaa.gov/products/CDB/CDB_Archive_html/bulletin_032015/), accessed 16 July 2015.]
- Bell, M. L., M. S. O'Neill, N. Ranjit, V. H. Borja-Aburto, L. A. Cifuentes, and N. C. Gouveia (2008), Vulnerability to heat-related mortality in Latin America: A case-crossover study in São Paulo, Brazil, Santiago, Chile and Mexico City, Mexico, *Int. J. Epidemiol.*, 37(4), 796–804, doi:10.1093/ije/dyn094.
- Bumbaco, K. A., K. D. Dello, and N. A. Bond (2013), History of Pacific Northwest heat waves: Synoptic pattern and trends, *J. Appl. Meteorol. Climatol.*, 52(7), 1618–1631, doi:10.1175/JAMC-D-12-094.1.
- Campetella, C. M., and N. E. Possia (2007), Upper-level cut-off lows in southern South America, *Meteorol. Atmos. Phys.*, 96(1), 181–191, doi:10.1007/s00703-006-0227-2.
- Caplan, P., J. Derber, W. Gemmill, S.-Y. Hong, H.-L. Pan, and D. Parrish (1997), Changes to the 1995 NCEP operational Medium-Range Forecast Model Analysis–Forecast System, *Weather Forecasting*, 12(3), 581–594, doi:10.1175/1520-0434(1997)012<0581:CTTNOM>2.0.CO;2.
- Damião Mendes, M. C., and I. F. Albuquerque Cavalcanti (2014), The relationship between the Antarctic oscillation and blocking events over the South Pacific and Atlantic Oceans, *Int. J. Climatol.*, 34(3), 529–544, doi:10.1002/joc.3729.
- Dinku, T., S. J. Conner, and P. Ceccato (2009), Comparison of CMORPH and TRMM-3B42 over mountainous regions of Africa and South America, in *Satellite Rainfall Applications for Surface Hydrology*, pp. 193–204, Springer, Netherlands.
- Eskridge, R. E., J. Y. Ku, S. T. Rao, P. S. Porter, and I. G. Zurbenko (1997), Separating different scales of motion in time series of meteorological variables, *Bull. Am. Meteorol. Soc.*, 78(7), 1473–1483, doi:10.1175/1520-0477(1997)078<1473:SDSOMI>2.0.CO;2.
- Fuenzalida, H., R. Sanchez and R. Garreaud (2005), A climatology of cut off lows in the Southern Hemisphere, *J. Geophys. Res.*, 110, D1801, doi:10.1029/2005JD005934.
- Garreaud, R., J. Rutllant, and H. Fuenzalida (2002), Coastal lows along the subtropical west coast of South America: Mean structure and evolution, *Mon. Weather Rev.*, 130(1), 75–88, doi:10.1175/1520-0493(2002)130<0075:CLATSW>2.0.CO;2.
- Garreaud, R. D. (2009), The Andes climate and weather, *Adv. Geosci.*, 22, 3–11.
- Garreaud, R. D., and P. Aceituno (2007), Atmospheric circulation and climatic variability, in *The Physical Geography of South America*, edited by A. Orme, T. T. Veblen, and K. Young, pp. 45–59, Oxford Univ. Press, U. K.
- Garreaud, R. D., and H. A. Fuenzalida (2007), The influence of the Andes on cutoff lows: A modeling study, *Mon. Weather Rev.*, 135(4), 1596–1613, doi:10.1175/MWR3350.1.
- Gimeno, L., R. M. Trigo, P. Riberia, and J. A. García (2007), Editorial: Special issue on cut-off low systems (COL), *Meteorol. Atmos. Phys.*, 96(1), 1–2, doi:10.1007/s00703-006-0216-5.
- Grotjahn, R. (2016), Western North American extreme heat, associated large-scale dynamics, and performance by a climate mode, in *Dynamics and Predictability of Large-Scale, High-Impact Weather and Climate Events*, edited by J. Li et al., pp. 198–209, Cambridge Univ. Press, Cambridge, U. K.
- Grotjahn, R., and G. Faure (2008), Composite predictor maps of extraordinary weather events in the Sacramento, California, region, *Weather Forecasting*, 23(3), 313–335, doi:10.1175/2007WAF2006055.1.
- Hakim, G. J. (2003), Cyclogenesis, in *Encyclopedia of Atmospheric Sciences*, edited by J. Holton, J. Curry, and J. Pyle, pp. 589–594, Academic Press, London.
- Houston, J. (2006), The great Atacama flood of 2001 and its implications for Andean hydrology, *Hydrolog. Process.*, 20(3), 591–610, doi:10.1002/hyp.5926.
- Hughes, M., and A. Hall (2010), Local and synoptic mechanisms causing Southern California's Santa Ana winds, *Clim. Dyn.*, 34(6), 847–857, doi:10.1007/s00382-009-0650-4.
- Klein, S. A., and D. L. Hartmann (1993), The seasonal cycle of low stratiform clouds, *J. Clim.*, 6(8), 1587–1606, doi:10.1175/1520-0442(1993)006<1587:TSCOL>2.0.CO;2.
- Ma, C. C., C. R. Mechoso, A. W. Robertson, and A. Arakawa (1996), Peruvian stratus clouds and the tropical Pacific circulation: A coupled ocean-atmosphere GCM study, *J. Clim.*, 9(7), 1635–1645, doi:10.1175/1520-0442(1996)009<1635:PSCATT>2.0.CO;2.
- Märker, M., F. Dangel, M. V. Soto, and G. Rodolfi (2012), Assessment of natural hazards and vulnerability in the Rio Copiapó catchment: A case study in the ungauged Quebrada Cinchado catchment, *Investig. Geogr. Chile*, 44, 17–28.
- Marques, R. F. C., and V. B. Rao (1999), A diagnosis of a long-lasting blocking event over the southeast Pacific Ocean, *Mon. Weather Rev.*, 127(8), 1761–1776, doi:10.1175/1520-0493(1999)127<1761:ADOALL>2.0.CO;2.
- Mechoso, C. R., et al. (2014), Ocean–cloud–atmosphere–land interactions in the southeastern Pacific: The VOCALS program, *Bull. Am. Meteorol. Soc.*, 95(3), 357–375, doi:10.1175/BAMS-D-11-00246.1.

- Meza, F. J. (2013), Recent trends and ENSO influence on droughts in northern Chile: An application of the standardized precipitation evapotranspiration index, *Weather Climate Extremes*, 1, 51–58, doi:10.1016/j.wace.2013.07.002.
- Middleton, N. J., and T. Sternberg (2013), Climate hazards in drylands: A review, *Earth Sci. Rev.*, 126, 48–57, doi:10.1016/j.earscirev.2013.07.008.
- Miky-Funatsu, B., M. A. Gan, and E. Caetano (2004), A case study of orographic cyclogenesis over South America, *Atmosfera*, 17(2), 91–113.
- Muggeo, V. M., and S. Hajat (2009), Modelling the non-linear multiple-lag effects of ambient temperature on mortality in Santiago and Palermo: A constrained segmented distributed lag approach, *Occup. Environ. Med.*, 66(9), 584–591, doi:10.1136/oem.2007.038653.
- Muñoz, R. C., and R. D. Garreaud (2005), Dynamics of the low-level jet off the west coast of subtropical South America, *Mon. Weather Rev.*, 133(12), 3661–3677, doi:10.1175/MWR3074.1.
- Nieto, R., L. Gimeno, L. de La Torre, P. Ribera, D. Gallego, R. García-Herrera, J. Agustín García, M. Nuñez, A. Redaño, and J. Lorente (2005), Climatological features of cutoff low systems in the Northern Hemisphere, *J. Clim.*, 18(16), 3085–3103, doi:10.1175/JCLI3386.1.
- Nieto, R., M. Sprenger, H. Wernli, R. M. Trigo, and L. Gimeno (2008), Identification and climatology of cut-off lows near the tropopause, *Ann. N. Y. Acad. Sci.*, 1146, 256–290, doi:10.1196/annals.1446.016.
- Pizarro, J. G., and A. Montecinos (2000), Cutoff cyclones off the subtropical coast of Chile, Preprints, Sixth Int. Conf. on Southern Hemisphere Meteorology and Oceanography, Santiago, Chile, Am. Meteorol. Soc., 278–279.
- Rahn, D., and R. Garreaud (2010), Marine boundary layer over the subtropical southeast Pacific during VOCALS-REx. Part II: Synoptic variability, *Atmos. Chem. Phys.*, 10, 4491–4505.
- Rahn, D. A. (2014), Observations of the marine boundary layer under a cutoff low over the southeast Pacific Ocean, *Meteorol. Atmos. Phys.*, 123(1), 1–15, doi:10.1077/s00703-013-0292-2.
- Reboita, M. S., R. Nieto, L. Gimeno, R. P. da Rocha, T. Ambrizzi, R. Garreaud, and L. F. Krüger (2010), Climatological features of cutoff low systems in the Southern Hemisphere, *J. Geophys. Res.*, 115, D17104, doi:10.1029/2009JD013251.
- Renwick, J. A., and M. J. Revell (1999), Blocking over the South Pacific and Rossby wave propagation, *Mon. Weather Rev.*, 127(10), 2233–2247, doi:10.1175/1520-0493(1999)127<2233:BOTSPA>2.0.CO;2.
- Rex, D. F. (1950), Blocking action in the middle troposphere and its effect upon regional climate. I. An aerological study of blocking action, *Tellus*, 2(4), 196–211, doi:10.1111/j.2153-3490.1950.tb00339.x.
- Ruttlant, J., and R. Garreaud (2004), Episodes of strong flow down the western slope of the subtropical Andes, *Mon. Weather Rev.*, 132(2), 611–622, doi:10.1175/1520-0493(2004)132<0611:EOSFDT>2.0.CO;2.
- Ruttlant, J. A., H. Fuenzalida, and P. Aceituno (2003), Climate dynamics along the arid northern coast of Chile: The 1997–1998 Dinámica del Clima de la Región de Antofagasta (DICLEIMA) experiment, *J. Geophys. Res.*, 108(D17), 4538, doi:10.1029/2002JD003357.
- Schulz, N., J. P. Boisier, and P. Aceituno (2012), Climate change along the arid coast of northern Chile, *Intl. J. Climatol.*, 32(12), 1803–1814, doi:10.1002/joc.2395.
- Stephens, G. (2005), Cloud feedbacks in the climate system: A critical review, *J. Clim.*, 18(2), 237–273, doi:10.1175/JCLI-3243.1.
- Tian, Y., C. D. Peters-Lidard, B. J. Choudhury, and M. Garcia (2007), Multitemporal analysis of TRMM-based satellite precipitation products for land data assimilation applications, *J. Hydrometeorol.*, 8(6), 1165–1183, doi:10.1175/2007JHM859.1.
- Trenberth, K. F., and K. C. Mo (1985), Blocking in the Southern Hemisphere, *Mon. Weather Rev.*, 113(1), 3–21, doi:10.1175/1520-0493(1985)113<0003:BITSH>2.0.CO;2.
- Urrutia, R., and C. Lanza (1993), *Catástrofes en Chile 1541–1992*, 440 pp., Editorial La Noria, Santiago.
- Valdés-Pineda, R., J. B. Valdés, H. F. Diaz, and R. Pizarro-Tapia (2015), Analysis of spatio-temporal changes in annual and seasonal precipitation variability in South America-Chile and related ocean-atmosphere circulation patterns, *Int. J. Climatol.*, doi:10.1002/joc.4532.
- Vargas, G., L. Ortíeb, and J. Ruttlant (2000), Aluviones históricos en Antofagasta y su relación con eventos El Niño/Oscilación del Sur, *Rev. Geol. Chile*, 27(2), 157–176, doi:10.4067/S0716-0208200000200002.